Astronomy Reports, Vol. 47, No. 4, 2003, pp. 333–342. Translated from Astronomicheskiĭ Zhurnal, Vol. 80, No. 4, 2003, pp. 364–373.

Meridional Drift of Large-Scale Solar Magnetic Fields

V. N. Obridko and B. D. Shelting

Institute of Terrestrial Magnetism, Ionosphere and Radio Wave Propagation, Troitsk, 142190, Russia

Received August 5, 2002; revised October 10, 2002

Abstract—It is shown that the meridional drift of large-scale fields starts in the equatorial zone and continues over 15–16 yrs (16–17 according to another estimate), i.e., during three fourths of the 22-year cycle. There is an abrupt retardation of the drift at latitudes of 30–50°, and a stagnation region arises, where the drift rate does not exceed several meters per second. The drift becomes rapid again at higher latitudes. The stagnation region coincides with the area in which the radial gradient of the rotational velocity is close to zero in the convective zone. This drift is compared with helio-seismological data on the rotation in the convective zone. A model is proposed taking into account some elements of dynamo theory. © *2003 MAIK "Nauka/Interperiodica".*

1. INTRODUCTION

The phenomenon of meridional drift, or more precisely, the displacement of zones of solar activity in latitude, was revealed virtually simultaneously with the discovery of solar cyclicity. While we recognize Schwabe's report of 1843 as the first indication of a possible 10-year periodicity, we can find the first statement about the drift of a zone of spots in Carrington's classical treatise of 1863. For a long time, it was considered to be obvious that both phenomena exhibit a single periodicity. We now know that, though the spots indeed appear at a fixed latitude with a period of 11 yrs (or closer to 10 yrs in the twentieth century), the lifetime for the spots of each cycle is significantly longer. The first spots of a new cycle appear at latitudes of 40° and higher several years before the solar minimum, while the last spots are sometimes observed after the solar minimum at latitudes of about 5–10°. Thus, the idea of an extended solar cycle was introduced [1].

The next step, namely the analysis of cyclic variations of the large-scale and background fields, was started only in the 1960s. There is no doubt that the periodicity of the large-scale fields at each latitude is close to the periodicity of local fields and sunspots. However, the latitude dependence is less clear. Some papers [2–14] indicate that the meridional drift is directed from the equator toward the poles, however, other papers [15–17] contest this. Finally, some papers of the former group (see, for example, [7]) admit a possible additional drift from middle latitudes toward the equator, along with the meridional drift from the middle latitudes toward the poles. The inconsistency of these findings is first and foremost connected with the difficulties of eliminating the effects of stronger local fields in the total signal. In addition, the solar rotation, whose velocity exceeds that of the meridional drift of the large-scale fields by two orders of magnitude, contributes greatly to Doppler measurements.

The comparatively short interval for which data on the magnetic fields of the entire solar disk are available represents another difficulty. Therefore, the very thorough works [18–20] analyze data for only 10 yrs, while [9, 21] consider data for 22 yrs.

Here, we study the meridional drift of the large-scale fields over a long time interval, paying particular attention to the identification of the large-scale fields. For our analysis, we use both magnetic-field data detected using various magnetographs over 40 yrs and unified into a single data set, and magnetic-field data recovered from Hα filament observations obtained over 85 yrs.

Since we are analyzing cyclic properties of the large-scale magnetic field, lower limits on the spatial size of the field are imposed by the observational technique used. In our analysis, the magnetograph data limit the spatial size of the field in three ways.

(1) The spatial resolution of the Stanford magnetograph is $3'$ ($\approx 0.2R_0$, where R_0 is the solar radius). Though other magnetographs provide higher resolution, the data were later averaged.

(2) The observations of magnetic fields at various latitudes were averaged over an entire Carrington revolution before the construction of the latitude–time diagrams.

(3) The number of harmonic coefficients used when calculating the magnetic-field components from the longitudinal field using Legendre polynomials was limited. We took into account only the first ten harmonics, which corresponds to sizes no smaller

1063-7729/03/4704-0333$24.00

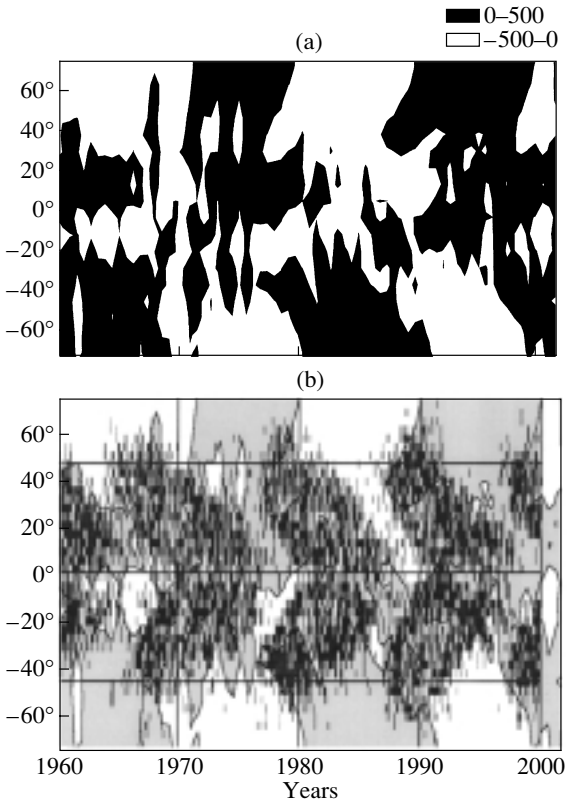

Fig. 1. (a) Latitude–time diagram for the radial magnetic field directly detected by magnetographs. (b) The same diagram combined with the Maunder butterflies.

than $0.2R_0$. This provides an additional limitation on the spatial size of the field.

For the Hα data, the second and third constraints apply in the same way. In addition, the technique used to recover the field from spectral heliograms reconstructs large-scale fields far from active regions. Since the field strengths are not used in the analysis, the contribution of strong local fields to the reconstructed fields is considerably diminished. Therefore, the reconstructed fields are the most convenient for studies of the meridional drift [22, 23].

In Section 2, we shall compare data on the localization of spots and on the drift of the large-scale magnetic field obtained from direct magnetograph measurements over 40 yrs, as well as with magnetic data reconstructed over 85 yrs. These data are subject to additional filtration in Section 3. A subsidiary analysis to ascertain the phase dependence and drift rate is presented in Section 4. Section 5 presents a discussion of the results.

2. COMPARING THE DRIFTS OF LOCAL AND LARGE-SCALE FIELDS

The first set of data obtained by magnetographs covers 40 yrs (1960–2002), and includes the Mount Wilson magnetic measurements over 1960–1978, Kitt Peak data over 1975–1984, and Stanford measurements from 1976 until the present time. All data were graciously made available by researchers of these observatories. We have unified these data into a single (WSO) system [24]. Using these data, we have constructed latitude–time diagrams for the *longitudinal* magnetic fields averaged over a Carrington revolution.

Guided by the widespread hypothesis that the large-scale field in the photosphere is radial, we can calculate the radial field and construct the corresponding diagram. The difference between the two diagrams is insignificant, except for a small strengthening of B_r in comparison with the longitudinal field in near-polar regions. Therefore, we present only the B_r diagram (Fig. 1a).

We can immediately see the fine structure of the field: a number of "tongues" and "bays", and, first and foremost, the seeming absence of a clear direction for the meridional drift, especially at low latitudes. The obvious reason is the absence of the third constraint above limiting the size of the fields from below. We observe the total field rather than the sum of its largest-scale components ($l \leq 9$). The contribution of intense, small-scale, local fields is strong. This is first manifest at low latitudes, where we find a superposition of two meridional drifts: from the equator toward the pole for the large-scale fields and from the middle latitudes toward the equator for the local fields.

Figure 1b combines in a single latitude–time diagram the magnetograph data on the large-scale magnetic fields and the Maunder butterflies for sunspots. We can see that the local fields visibly *disrupt* the continuous drift of the large-scale fields from the equator toward the pole.

The Hα data on the large-scale fields covers 85 yrs (1915–2000). These data are partially taken from the atlas of P. McIntosh (1964–1974), while the remaining are published or presented to us directly by Sivaraman and Makarov (1975–2000). As is discussed above, when working with the Hα data, we used an original technique to derive the magnetic-field strength from the synoptic maps, which specify only the sign of the magnetic field. To ensure the values were reasonable, we compared directly measured magnetic-field strengths with those calculated from the Hα observations for overlapping time intervals [24].

A *direct* study of the polarity of the large-scale fields recovered from Hα data (i.e. without computing the radial field via polynomials) was carried out in [12]. As expected, the meridional drift toward the pole became much clearer in comparison with the magnetograph data. The drift toward the equator became almost invisible, being manifest only in small "tongues"

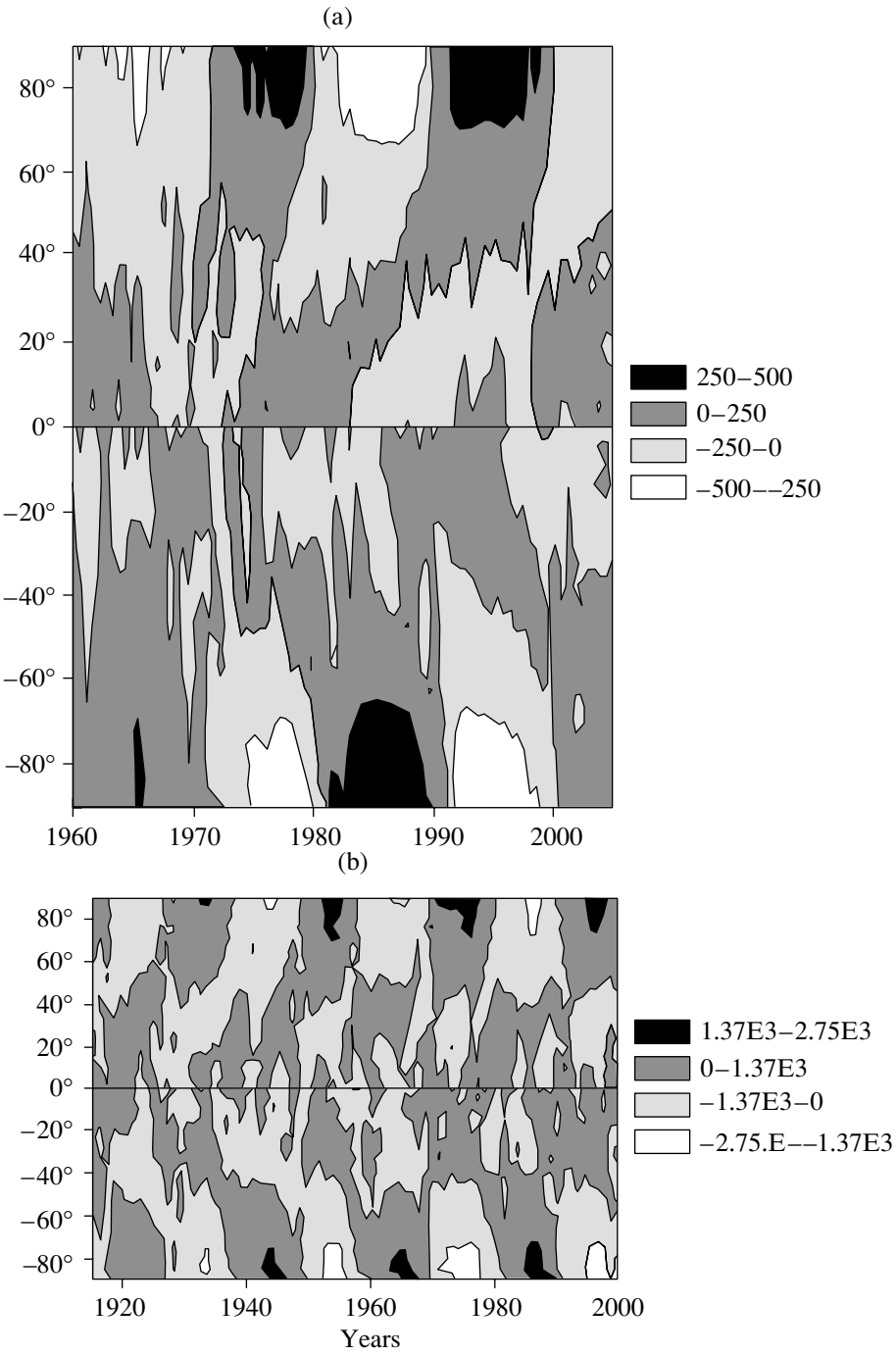

Fig. 2. Latitude–time diagram for the radial magnetic field calculated in the potential approximation from the (a) magnetograph and (b) Hα data.

of the secondary polarity near the equator. Nevertheless, more careful filtering is obviously necessary.

3. CALCULATIONS OF CYCLIC VARIATIONS OF RADIAL FIELDS IN THE PHOTOSPHERE

The calculations of each component of the magnetic field in the photosphere from the detected longitudinal field are carried out in a potential approximation. The harmonic coefficients are obtained by two different techniques: the method of orthogonal Legendre polynomials [25] and the least squares method [26]. The radius of the source surface is assumed to be $2.5R_0$. A "classical" approximation was used; i.e., radial structure for the field was not assumed *a priori*. Since we were mainly interested in the behavior of

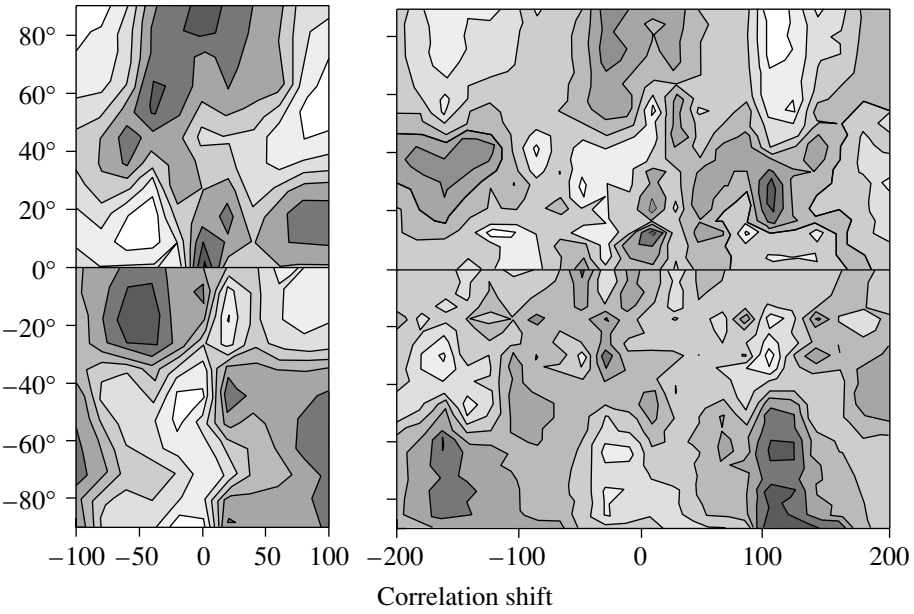

Fig. 3. Correlation between the large-scale magnetic fields obtained for various latitudes from the magnetograph (left) and Hα (right) data.

the radial component B_r of the magnetic field, we first calculated the daily radial field values for latitudes from 0° to ±90° in steps of 1/15 in the sine of the latitude for the whole time interval. The results were then averaged over a Carrington revolution. We subsequently combined all data into a single file and constructed the latitude–time diagrams. Let us examine these in detail (Figs. 2a, 2b).

Figure 2a presents the latitude–time diagram for the radial magnetic field B_r calculated from the direct measurements of the large-scale longitudinal magnetic field. Figure 2b shows the latitude–time diagram for the B_r calculated from the Hα measurements of the large-scale longitudinal magnetic field. Let us analyze these two plots jointly. The dark gray regions that shade into black near the poles correspond to N polarity of the magnetic field (>0), while the light gray regions that shade into white near the poles correspond to S polarity (<0).

The motion of regions of large-scale magnetic field of each polarity from the equator toward the poles is clearly visible (compare with Fig. 1a). This drift of the large-scale fields differs fundamentally from the drift of the local fields, in particular from the motion of the Maunder butterflies from middle latitudes toward the equator. The drift rate of the large-scale fields depends on the latitude. From the equator to latitudes of 20–25°, the drift is fairly rapid, and the magnetic field passes through this interval in two to three years. At latitudes of 25–50°, the drift rate sharply decreases (it does not exceed 1 m/s), and the magnetic field passes through this 25° interval in 15 yrs. Further, the drift rate rapidly increases near the pole, and the magnetic field passes through the remaining 40–50° in about one year. Thus, the total time for the transport of the large-scale fields is approximately 17–18 yrs, i.e., there is an extended cycle. It is interesting that the centers of the regions of the large-scale fields of each polarity are always situated near maxima of the local field at the equator and minima of the local field at the poles. Each regular region of large-scale field of a certain polarity arises at the equator when there is a reversal of the polarity of the two preceding fields at the poles (the last field, with the same polarity as the current equatorial field, and the next field, with the opposite polarity). The width of the region of each polarity in time is 11 yrs. During this time interval, three regions of large-scale field of alternating polarity corresponding to three different cycles lie one above the other at latitudes from the equator to the poles. Recall that the extended cycle of the local fields lasts 12–13 yrs, and there is a partial overlapping of two neighboring cycles at the latitudes of the wings of the Maunder butterflies. Note also that the maximum strength of the local fields is observed in a narrow latitude interval near 20°, whereas the maximum strength for large-scale fields is observed near the poles.

Comparing these large-scale field diagrams with the Maunder butterflies, we arrive at the following conclusions.

(1) There is a clear, mutually opposite motion of the large-scale and local fields: the large-scale fields move from the equator toward high latitudes, while

the local fields move from the high latitudes toward the equator. In each activity cycle, the local fields arise before the polarity reversal of the large-scale fields (by two to three years), and disappear near the equator simultaneous with the next polarity reversal of the large-scale fields, covering a time interval of 12–13 yrs. The narrow intersection of these two regions occurs at latitude 20°.

(2) The inclination of the butterflies to the time axis is virtually constant (a linear approximation is good) during their entire motion from the middle latitudes toward the equator. This inclination is about 5° per year. A butterfly moves through its whole path over 10–11 yrs, from the minimum of each cycle to the minimum of the following cycle. The central area of the butterfly (where there is the greatest number of spots) corresponds to the maximum of the local cycle, and coincides in latitude (20°) with the intersection of the diagrams of the local and large-scale fields. The behavior of the large-scale fields differs from that of the local fields. First, the drift rate is not constant during the whole time interval, as was indicated above. Second, the large-scale fields move through their path from the equator to the middle latitudes, on average, over a longer time of about 17 yrs; i.e., from the maximum of the local cycle nearly to the minimum of the cycle following the next (the time is short by only one to two years).

These conclusions agree with the results presented in Fig. 3, which shows the correlations between the large-scale magnetic fields at various latitudes. The cross-correlation of the equatorial radial field with the radial field at other latitudes is calculated. We can see that the correlation region extends from the equator to the poles, and its total length exceeds 200 Carrington revolutions, or 15 yrs. Similar findings are presented in [14].

4. GENERAL SCHEME FOR THE MERIDIONAL CIRCULATION OF THE LARGE-SCALE MAGNETIC FIELDS

To ascertain the drift characteristics obtained from the magnetograph data, we approximate the field distribution in the latitude–time diagram (see the northern hemisphere in Fig. 2a) using the function

$$B_r/\sigma(\vartheta) = \sum_{\omega} A_\omega(\vartheta)\exp(i\omega(t+\varphi(\vartheta))), \qquad (1)$$

$$\sum_{\omega} A_\omega^2 = 1. \qquad (2)$$

We use this form of the Fourier transformation in order to analyze specifically the meridional drift, and to separate it from the latitudinal variations of the strength of large-scale fields. Therefore, we first calculate the average $\langle B_r\rangle$ and variance $\sigma(\theta)$ over the entire time interval (1960–2002) for the each latitude. The average $\langle B_r\rangle$ turns out to be close to zero (as was expected), and all the $B_r(\theta,t)$ are then normalized to the corresponding $\sigma(\theta)$. Further, the amplitude $A_\omega(\theta)$, frequency ω, and phase $\varphi(\theta)$ are found for each latitude via a Fourier-series expansion with fractional harmonics. As was mentioned above, the frequency ω corresponding to the maximum (about 20 yrs) is virtually independent of latitude and equal to 8.706 rad/s (i.e., the period is 20.87 yrs). We shall call this the "22-year cycle" and denote the related parameters by the subscript 22. The phase corresponding to this period is a rather complicated function of θ, accurate to within an arbitrary initial value.

Figure 4 presents the function $\varphi(\theta)$, which can be

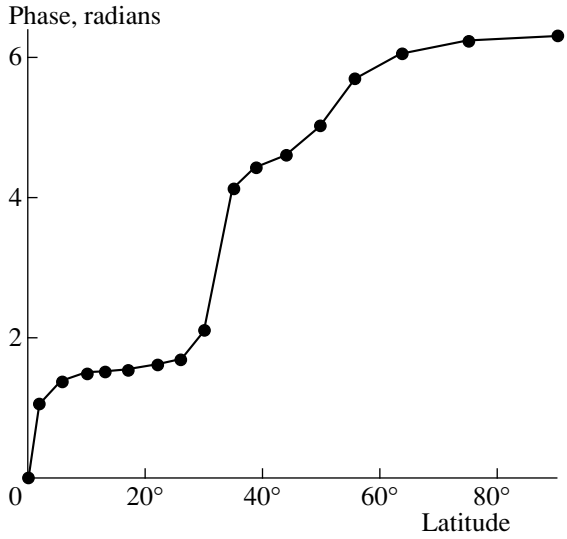

Fig. 4. Phase of the meridional drift model as a function of latitude.

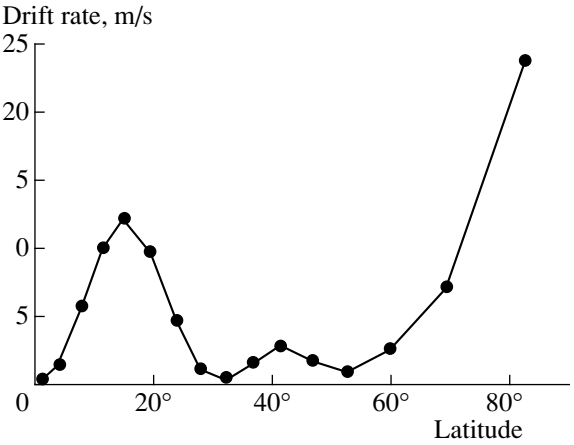

Fig. 5. The model rate for the meridional drift of the large-scale magnetic fields.

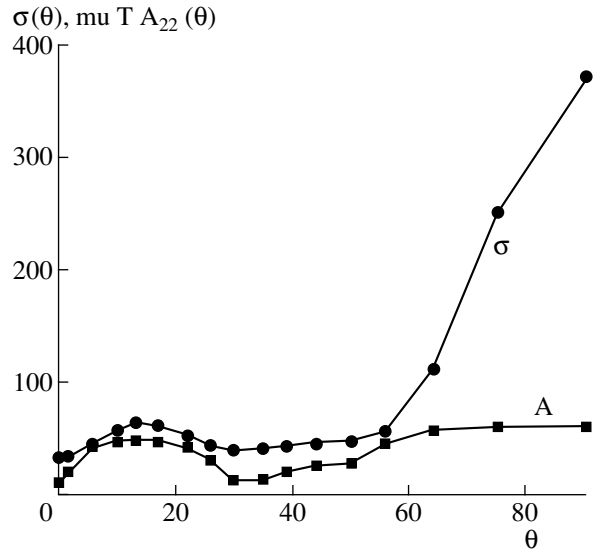

Fig. 6. The variance and amplitude of the 22-year cycle as functions of latitude in the model for the meridional drift.

easily recalculated to give the rate of the meridional drift, shown in Fig. 5. Figure 5 indicates that there are two regions of rapid drift. The drift rate grows from almost zero near the equator and reaches its maximum of 13 m/s at a latitude of 20°. Approximately the same rate was obtained in [13, 27, 28]. At higher latitudes from 33° to 53°, the rate is extremely small, 1–3 m/s. Further, the rate rapidly increases to 25 m/s near the pole.

Table 1. Quantitative characteristics of the drift of the large-scale magnetic fields

Latitude	$A(\theta)$	$A^2(\theta)$	$\sigma(\theta)$	Phase
90°	0.6226	0.3877	374.8899	6.31828
75°	0.6227	0.3878	251.5153	6.2448
64°	0.5932	0.3518	113.0285	6.06852
56°	0.4574	0.2092	57.6674	5.71597
50°	0.2950	0.0871	47.2941	5.01434
44°	0.2659	0.0707	46.7928	4.62862
39°	0.2240	0.0502	44.6023	4.42442
35°	0.1384	0.0191	41.5526	4.14342
30°	0.1331	0.0177	40.0913	2.11691
26°	0.3148	0.0991	44.7899	1.72671
22°	0.4302	0.1851	53.7202	1.62887
17°	0.4881	0.2383	63.0929	1.56958
13°	0.4976	0.2476	63.6749	1.53136
10°	0.4865	0.2366	58.8488	1.49697
6°	0.4236	0.1795	47.0516	1.41616
2°	0.2190	0.0480	36.1304	0.02248
0°	0.1108	0.0123	34.9017	0.000

The functions $\sigma(\theta)$ and $A_{22}(\theta)$ (Fig. 6) also indicate these two zones. The function $\sigma(\theta)$ is the r.m.s magnetic field calculated for a given latitude over the long time interval of two magnetic cycles. We can see that the r.m.s. strength of the large-scale field in the polar zone exceeds that of the equatorial maximum at latitudes 16°–18° by a factor of five or more. The function $A_{22}(\theta)$ describes the contribution of the 22-year cycle at each latitude. Here, these two maxima are also seen, but the difference between them is much smaller. The value of $A_{22}(\theta)$ at high latitudes exceeds that at latitude 20° by only 25%.

The quantitative results of the foregoing analysis are presented in the Table.

Figure 7 shows a scheme for the cyclic variation of the meridional drift obtained by the formula

$$B_r = A_{22}(\vartheta)\exp(i\omega_{22}(t+\varphi_{22}(\vartheta))).$$

This means that we use here two additional types of filtering besides the three previous types presented in the Introduction. First, we add frequency filtering to eliminate every cycle except the 22-year cycle. Second, we remove the strong dependence of the large-scale fields on latitude, expressed in Eq. (1) by the denominator $\sigma(\theta)$.

5. DISCUSSION

The drift of the large-scale fields from the equatorial zone toward the pole takes 15–16 yrs (or 16–17 yrs according to another estimate), i.e., three fourths of the 22-year cycle. The reverse motion, which is not directly observed, takes 5–6 yrs. The drift on the surface during these 5–6 yrs is virtually equal to zero. It then abruptly grows, and its rate exceeds 10 m/s. There is an abrupt retardation of the drift at latitudes 30–50°, and a stagnation region arises, where the rate does not exceed several meters per second. The drift again becomes rapid at higher latitudes. The stagnation region coincides with the region where the radial gradient of the rotational velocity in the convective zone is close to zero (there is a change of sign in $\partial\omega/\partial r$). At the same time, the stagnation region is extended in latitude, and its high-latitude and low-latitude boundaries appear as neutral curves in the latitude–time diagrams. The variation of these boundaries and its secular cycle were studied in [29, 30].

The average rate of the polar drift is ~ 2 m/s.

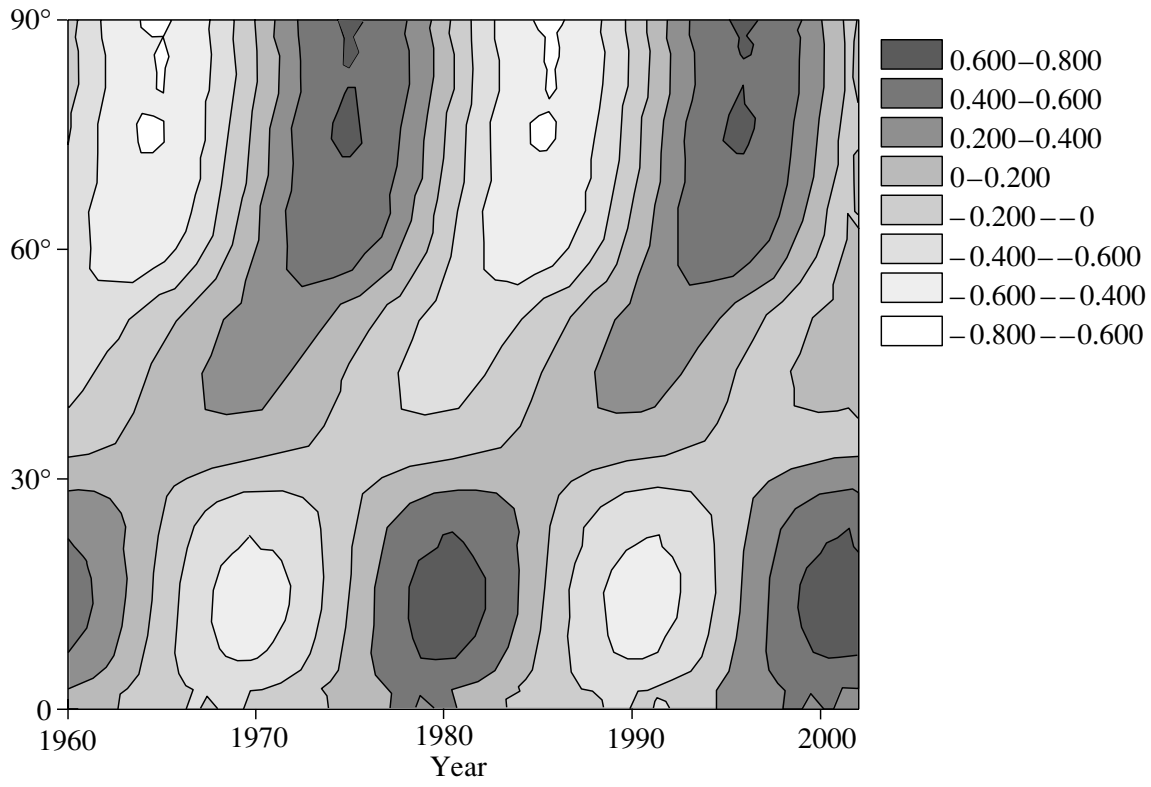

Fig. 7. Scheme for the cyclic variation of the meridional drift.

Let us consider the agreement between these findings and classical dynamo models. In most models (see, for example, [31] using the model of the convective zone [32]), the meridional drift naturally arises in the generation process due to the negative dynamo number at the base of the convective zone. This drift is directed toward the equator, and explains the Maunder butterflies for the local fields. These models neglect drift motions in higher layers of the convective zone [33]. The meridional drift of the large-scale fields toward the pole is frequently explained as a consequence of the diffusion of tail polarities of the local fields due to differential rotation (see [10, 11] and references therein). However, in this case, it is difficult to understand why the equatorial fields follow the evolution of the polar fields with a time lag of 5–6 yrs (see [29] and references therein). There are also other direct objections to this scheme with the diffusion transport of some portion of the local fields toward the pole. It is unclear how the large-scale, deep, poloidal magnetic field can originate from surface elements in the form of sunspots [34, 35]. Finally, it remains unclear why the large-scale fields in the polar zone significantly (by a factor of five or more) exceed the equatorial large-scale fields in the case of simple transport of the tails of active regions toward the pole. A flux of material directed toward the pole is postulated in [18, 19], where it is shown that the calculated drift can agree with observations for appropriately chosen parameters. However, the time interval used for the comparison with observations is short, and the polar drift covers only 10 yrs.

One qualitative scheme for the generation of large-scale fields in the solar cycle is the following. We will describe it in terms of the concentrated fields (CF) and diffusive fields (DF) introduced in [18], which we consider to be more convenient from the physical point of view than the terms toroidal and poloidal fields that are usually used in dynamo theory.

We shall use the structure of motions in the convective zone described in [32]. Figures 8a and 8b show the important $d\Omega/dr$ and $d\Omega/d\theta$ diagrams. The strongest radial gradient takes place within a narrow layer of thickness $0.05R_0$ [36] situated directly beneath the base of the convective zone at latitudes lower than 36° ($\sin\theta < 0.6$). This is the tachoclinic region where the $\alpha - \omega$ dynamo operates [37]. Here, the ω dynamo creates strong concentrated fields. Since $\alpha < 0$ in this region [31], this region of CF drifts from the middle latitudes toward the equator, while the fields rapidly (over several days) rise to the surface radially due to the buoyancy force. These fields are tubes of CF, with their meridional drift during their ascent being insignificant. For a meridional drift rate of 10 m/s, the tube drift toward the pole over

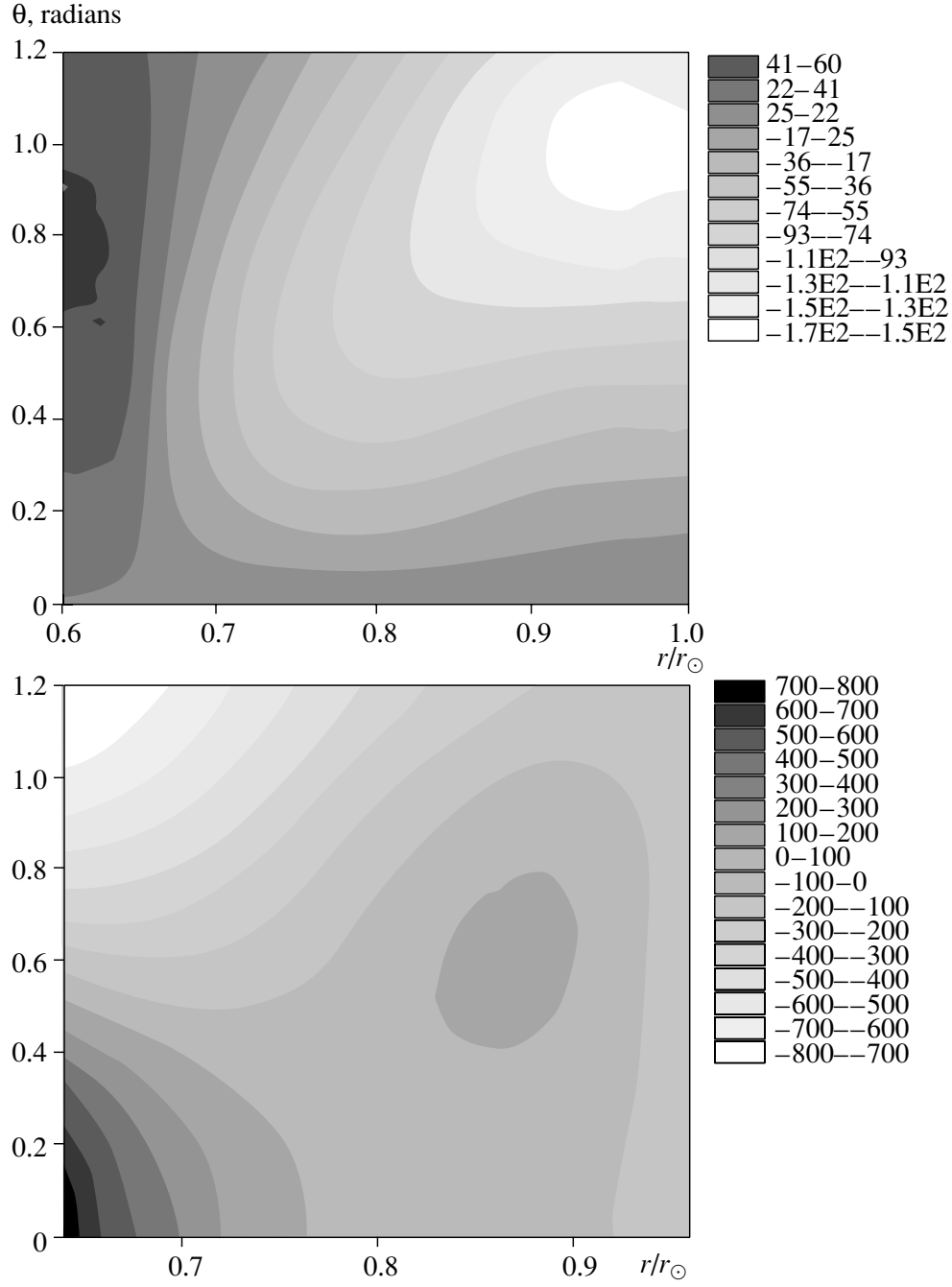

Fig. 8. $d\Omega/dr$ (top) and $d\Omega/d\theta$ (bottom) diagrams.

15 days does not exceed 10^4 km, remaining less than the size of the tube itself. As a result, we observe on the surface Maunder butterflies directed toward the equator, reflecting the drift of the "spot creating" zone in the tachoclinic region. However, the spot tubes are not directly connected to the tachoclinic region, and are immersed below the solar surface no deeper than 6–12 000 km [34, 35]. The sunspots thus remain surface phenomena.

The α (or α^2) dynamo operates simultaneously [38, 39]. It is more efficient in higher layers, where the parameter α changes sign for $R \geq 0.72R_0$ [31]. The evolution of diffuse fields is independent of the CFs [18], since the equation for weak, large-scale DFs branches off. The ω dynamo wave becomes the lower boundary condition for the α dynamo. Thus, the DFs arise in a wider region of the convective zone, rather than in the narrow tachoclinic region. There are no sharp boundaries for these fields, and the magnetic-pressure gradients are weak. Therefore, these fields

move along with the medium. They rise slowly (they have low buoyancy) and are strongly dragged by the meridional drift in the convective zone. These fields can be additionally strengthened in the polar region due to the strong negative gradient $d\Omega/d\theta$ (Fig. 8b). The rates of the meridional drift obtained in [33] from helio-seismological data agree well with our results. Though the DFs arise above the CFs, they must be considered as being deeper when interpreting the observations. Therefore, we usually treat the large-scale and global magnetic fields as deep phenomena (see the discussion in [14]).

Stix [40] has calculated a similar pattern for the drift of the large-scale fields toward the pole using an $\alpha\Omega$ dynamo model.

It is extremely difficult to reveal the reverse drift in both our data and the helio-seismological data. The analysis of the cross-correlation of the large-scale field strengths in [14] does not indicate any direct drift, but shows that the equatorial structure is similar to the polar structure with a time lag of 5–6 yrs. This implies a rate for the reverse drift of ~ 5–6 m/s. Giles [33] likewise was not able to demonstrate the presence of a reverse drift directly using helio-seismological data, but estimated from the continuity equation the reverse rate to be ~ 3 m/s and the level in the convective zone where the meridional flow toward the pole is changed to the reverse flow to be $\sim 0.80R_0$.

In our discussion, we have used a model for the convective zone constructed especially for the rising branch of the 23rd cycle. If this model is changed, some of our results will require refinement.

All our calculations have used a "classical" model in which the source surface is $2.5R_0$ from the Sun's center, and the field at the surface of the photosphere is potential. The calculations in an alternative model in which the photospheric field is taken to be radial and the source surface is at $3.25R_0$ give no significantly new results. The diagram obtained is virtually the same as that in Fig. 2a.

6. ACKNOWLEDGEMENTS

The authors are grateful to E. V. Ivanov, K. M. Kuzanyan, and D. D. Sokolov for helpful discussions, to V. I. Makarov and A. G. Tlatov for providing us with unpublished data, and to the Wilcox Solar Observatory staff for the data received via INTERNET. This work was supported by the Russian Foundation for Basic Research (project codes 00-15-96661 and 02-02-16199) and by INTAS (project 2000-840).

REFERENCES

1. K. Harvey, in *The Solar Cycle* , Ed. by K. L. Harvey, Astron. Soc. Pac. Conf. Ser. **27**, 335 (1992).
2. V. Bumba and R. Howard, Astrophys. J. **141**, 1502 (1965).
3. T. L. Duvall, Jr., Sol. Phys. **63**, 3 (1979).
4. R. Howard and B. J. LaBonte, Sol. Phys. **74**, 131 (1981).
5. B. J. LaBonte and R. F. Howard, Sol. Phys. **80**, 361 (1982).
6. V. I. Makarov and K. R. Sivaraman, Sol. Phys. **119**, 35, (1989).
7. V. I. Makarov, M. P. Fatianov and K. P. Sivaraman, Sol. Phys. **85**, 215 (1983).
8. R. K. Ulrich, J. E. Boyden, L. Webster, *et al.*, Sol. Phys. **117**, 291 (1988).
9. Y.-M. Wang, J. Lean, and N. R. Sheeley, Geophys. Res. Lett. **27**, 505 (2000).
10. Y.-M. Wang, A. G. Nash, and N. R. Sheeley, Astrophys. J. **347**, 529 (1989).
11. Y.-M. Wang, A. G. Nash, and N. R. Sheeley, Science **245**, 712 (1989).
12. V. N. Obridko and G. Gaziev, in *The Solar Cycle* , Ed. by K. L. Harvey, Astron. Soc. Pac. Conf. Ser. **27**, 410 (1992).
13. R. W. Komm, R. F. Howard, and J. W. Harvey, Sol. Phys. **147**, 207(1993).
14. E. V. Ivanov and V. N. Obridko, Sol. Phys. **206**, 1 (2002).
15. M. Perez Garde, M. Vazquez, H. Schwan, and H. Wohl, Astron. Astrophys. **93**, 67 (1981).
16. B. N. Anderson, Sol. Phys. **94**, 49. (1984).
17. G. Lustig and H. Wohl, Astron. Astrophys. **229**, 224. (1990).
18. M. Dikpati and A. R. Choudhuri, Astron. Astrophys. **291**, 975. (1994).
19. M. Dikpati and A. R. Choudhuri, Sol. Phys. **161**, 9 (1995).
20. A. R. Choudhuri and M. Dikpati, Sol. Phys. **184**, 61 (1999).
21. Y.-M. Wang, N. R. Sheeley, Jr., and J. Lean, Geophys. Res. Lett., **27**, 621 (2000).
22. V. N. Obridko and B. D. Shelting , Sol. Phys. **201**, 1 (2001).
23. B. D. Shelting and V. N. Obridko, Astron. Astrophys. Trans. **20**(3), 491 (2001).
24. V. N. Obridko and B. D. Shelting , Sol. Phys. **184**, 187 (1999).
25. J. T. Hoeksema and P. H. Sherrer, *Solar Magnetic Field "— 1976 through 1985* (WCDA, Boulder, 1996).
26. K. G. Ivanov and A. P. Kharshiladze, Geomagn. Aeron. **34**, 22 (1994).
27. R. K. Ulrich, in *IAU Colloq. 137: Inside the Stars* (A93-53126 23-90, 1993), p. 25.
28. H. B. Snodgrass, Sol. Phys. **94,** 13 (1984).
29. V. I. Makarov, A. G. Tlatov, D. K. Callebaut, *et al.*, Sol. Phys. ,**198,** 409 (2001).
30. V. I. Makarov, A. G. Tlatov and K. R. Sivaraman, Sol. Phys. **202**, 11 (2001).

31. G. Belvedere, K. M. Kuzanyan, and D. D. Sokoloff, Mon. Not. R. Astron. Soc. **315**, 778 (2000).
32. J. Shou *et al.*, Astrophys. J. **505**, 390 (1998) .
33. P. M. Giles, *Time-Distance Measurements of Large-scale Flows in the Solar Convection Zone*, Dissertation, Stanford University (1999).
34. V. N. Obridko, *Sun Spots and Activity Complexes* [in Russian] (Nauka, Moscow, 1985).
35. J. Zhao, A. G. Kosovichev, and T. L. Duvall, Jr., Astrophys. J. **557**, 384 (2001).
36. A. G. Kosovichev, Astrophys. J. **469**, L61 (1996).
37. E. A. Spiegel and J. P. Zahn, Astron. Astrophys. **265**, 106 (1992).
38. H. K. Moffat, in *Magnetic Field Generation in Electrically Conducting Fluids* (Cambridge Univ., Cambridge, 1978).
39. F. Krause and K.-H. Radler, in *Mean Field Magnetogydrodynamics and Dynamo Theory* (Pergamon, Oxford, 1980).
40. M. Stix, Astron. Astrophys. Trans. **20**(3), 417 (2001).

Translated by V. Badin